Supplementary Data

Online single particle measurement of fireworks pollution during Chinese New Year in Nanning -Supplementary Information

Jingyan Li[1], Tingting Xu[1], Xiaohui Lu[1], Hong Chen[1], Sergey A. Nizkorodov[2], Jianmin Chen[1,3], Xin Yang[1,3,*], Zhaoyu Mo[4], Zhiming Chen[4], Huilin Liu[4], Jingying Mao[4], Guiyun Liang[4]

1. Shanghai Key Laboratory of Atmospheric Particle Pollution and Prevention, Department of Environmental Science and Engineering, Fudan University, Shanghai 200433, China. E-mail: jingyanli12@fudan.edu.cn
2. Department of Chemistry, University of California, Irvine, California 92697, United States
3. Fudan-Tyndall Center, Fudan University, Shanghai 200433, China
4. Guangxi Academy of Environmental Sciences, Nanning 530022, China

----

* Corresponding author. E-mail: yangxin@fudan.edu.cn

1. Satellite data

Figure S1 illustrates the pathways of air masses arriving at Nanning (a) and the stability of atmosphere (b) during the sampling period calculated from satellite data. The Hybrid Single Particle Lagrangian Integrated Trajectory (HYSPLIT) model (http://ready.arl.noaa.gov/HYSPLIT.php) was run in a 48-hour back-trajectory mode at 500 m to analyze the potential sources for the sampled air masses. Nanning is a city located in the southwestern part of China and is nearly 150 km away from the South Sea. During the sampling period, the air masses originated from the South Sea on all sampling days except on 4-Feb-2014. Air masses from open sea area are usually enriched with sea-salt particles and

can help to dilute polluted air mass. On 4-Feb-2014, the air mass originated from Yunnan Province, passed through inland residential and industrial areas and arrived at Nanning. The three-hour resolved Planetary Boundary Layer (PBL) height and Scaled Vertical Mixing Coefficient (SVMC) were obtained from the Global Data Assimilation System (GDAS) model (http://www.ready.noaa.gov/READYamet.php) and shown in **Fig. S1b.** Distinct diurnal variations of PBL height and SVMC can be observed from the figure. During the sampling period, PBL height rose around 7:00 a.m. every day and maintained at high value (>1000km) in day time, providing good conditions for mixing. After 18:00, both PBL height and SVMC dropped down quickly and kept at low values, indicating stagnant conditions established and maintained through nighttime.

2. The classification of particles

Organic carbon (OC) clusters were identified with strong organic makers in positive mass spectra, such as $^{27}C_2H_3^+$, $^{43}C_2H_3O^+$, $^{51}C_3H_4O^+$, $^{55}C_3H_3O^+$, $^{63}C_5H_3^+$, $^{74}C_3H_6O_2^+$, etc. Elementary carbon (EC) particles included series of carbon clusters:$^{12\sim144}C_n^{\pm}$(n=1-12). Elementary carbon and organic carbon (ECOC) particles, the mixture of EC and OC, featured similar peak intensities of $^{36}C_3^+$ and $^{37}C_3H^+$. Dust particles contained peaks of silicon ($^{59}SiO_2^-$ and $^{76}SiO_3^-$) and common metals existing in lithosphere ($^{24}Mg^+$, $^{27}Al^+$, $^{40}Ca^+$). Sea-salt particles were identified by ions containing sodium and chlorine ($^{23}Na^+$, $^{81/83}Na_2Cl^+$ and $^{35}Cl^-$). Ash/Metal particles contained peaks of potassium and chlorine ($^{39/41}K^+$, $^{113/115}K_2Cl^+$, $^{35/37}Cl^-$ and $^{109/111}K(Cl)_2^-$) and a variety of heavy metals, as discussed below. K-rich particles contained a prominent potassium ($^{39/41}K^+$) peak.

2.1 Classification of firework-related particles

Fireworks-Metal particles contained trace metals including strontium ($^{88}Sr^+$), barium ($^{138}Ba^+$, $^{154}BaO^+$), aluminum ($^{27}Al^+$) , manganese ($^{55}Mn^+$), copper ($^{63/65}Cu^+$) and lead ($^{206/207/208}Pb^+$). Strong ions of potassium ($^{39}K^+$), chlorine ($^{35/37}Cl^-$) and nitrate ($^{46}NO_2^-$, $^{62}NO_3^-$) were also observed, which mainly originated from black powder ingredients. Sr and Ba are considered to be good tracers for firework displays (Moreno et al., 2007; Huang et al., 2012).

Ash are potassium-rich particles intermixed with chlorine ($^{39}K^+$, $^{35/37}Cl^-$, $^{113/115}K_2Cl^+$, $^{109/111}KCl_2^-$), nitrate ($^{46}NO_2^-$, $^{62}NO_3^-$) and sulfate ($^{48}SO^-$, $^{64}SO_2^-$, $^{80}SO_3^-$, $^{96}SO_4^-$). The mass concentration of potassium and chlorine were previously found to increase significantly during the firework displays (Kulshrestha et al., 2004; Cheng et al., 2014). Particles containing potassium chloride and potassium nitrate fragments ($^{140}K_2NO^+$, $^{147}KNO_3NO^-$,

^{163}K(NO$_3$)$^-$) were identified as fireworks family by ATOFMS (Jeong et al., 2011; McGuire et al., 2011).

Dust particles were merged from two subtypes: MgAlSi and CaSi because they shared similar time variations and particle diameter distributions. MgAlSi particles had prominent ions of magnesium (^{24}Mg$^+$) and aluminum (^{27}Al$^+$ and ^{59}AlO$_2^-$) and less prominent ions of silicon (^{76}SiO$_3^-$, ^{60}SiO$_2^-$). Mg and Al are used as alloy magnalium (50:50 Mg:Al) for sparks and crackling stars in fireworks. Elements of Mg, Al were found to increase during firework displays in previous studies (Joly et al., 2010). CaSi particles are enriched with ions of silicon (^{76}SiO$_3^-$, ^{60}SiO$_2^-$) and calcium (^{40}Ca$^+$), which are believed to closely related to crustal compounds. Soil dusts are usually added during manufacturing fireworks/crackers to prevent accidental explosion. Also, severe explosion of fireworks could lead to the re-suspension of road dust (Tian et al., 2014).

OC-Sulfate cluster is featured by the organic fragments mentioned above and strong signals of sulfate (^{97}HSO$_4^-$). OC particles containing high intensity of sulfate signal (^{97}HSO$_4^-$) were recognized as freshly-emitted particles before, due to a relatively small coating of nitrate or ammonium compounds (Sullivan and Prather, 2007; Moffet et al., 2008).

Biomass Burning particles included prominent peaks of potassium ^{39}K$^+$, organo-nitrogen compounds (^{26}CN$^-$, ^{42}CNO$^-$), chlorine (^{35}Cl$^-$) and fragments of levoglucosan (^{45}CH$_2$O$^-$, ^{59}C$_2$H$_3$O$^-$ and ^{73}C$_3$H$_4$O$_2^-$), which agrees well with the particles associated with biomass burning in laboratory studies (Silva et al., 1999; Huo et al., 2016).

2.2 Classification of non-firework-related particles

OC group consists of OC-Sulfate, OC-Nitrate and HMOC. OC-Nitrate particles have similar positive mass pattern as OC-Sulfate, but exhibit higher intensity of nitrate (^{46}NO$_2^-$, ^{62}NO$_3^-$) ions. Usually, the difference between the intensities of sulfate ^{97}HSO$_4^-$ and nitrate (^{62}NO$_3^-$ and ^{125}H(NO$_3$)$_2^-$) in negative mass spectrum on OC containing particles indicate different atmospheric processes (Moffet et al., 2008). This subtype might originate from the night-time condensation of nitric acid on OC particles. High Mass Organic Carbon (HMOC) is distinguished by specific organic fragments in high m/z region (m/z 100-200). Specific peaks can be seen at m/z 115, 139, 142, 153, 165, 182, 189 and 202 in the positive ion mode mass spectra. It is important to note that ^{63}C$_5$H$_3^+$, ^{115}C$_9$H$_7^+$, ^{165}C$_{13}$H$_9^+$ and ^{189}C$_{15}$H$_9^+$ are markers for poly-aromatic species including PAH (Silva and Prather, 2000). HMOC can originate either from primary sources such as solid fuel combustion or from secondary processes. Considering that the diameters of HMOC particles were larger than 0.8 μm, the

HMOC cluster detected in our study were likely produced from ageing processes. Similar ion peaks and particle diameter distributions were previously observed and believed to be associated with HULIS species formed by fog processing (Qin and Prather, 2006).

Sea-salt particles show intense signals of sodium ($^{23}Na^+$) and characteristic sea salt signature ($^{81/83}Na_2Cl^+$). Lower intensities of chlorine peaks ($^{35/37}Cl^-$) and higher intensities of nitrate peaks ($^{46}NO_2^-$ and $^{62}NO_3^-$) indicate that atmospheric aging process had modified the composition of sea-salt particles during transport(Spencer et al., 2008). The sea-salt particle counts peaked in the afternoons on Jan-31 and Feb-1(**Fig. 5**) when wind blew from the South Sea (**Fig. 1**).

Industrial-Metal cluster featured peaks of iron ($^{54/56}Fe^+$), vanadium ($^{51}V^+$, $^{67}VO^+$) and strong peaks of phosphate ($^{79}PO_3^-$). Iron and vanadium rich particles have already been detected around integrated steelworks in London (Dall'Osto et al., 2008). Industrial particles observed in Shanghai showed high peak at $^{79}PO_3^-$ (Tao et al., 2011). Besides, the concentration of Industrial-Metal cluster kept relatively low during whole sampling period but appeared as spikes in coincidence with well-mixed ECOC, implying those two clusters might be contributed to by regional transport from industrial sources.

K-rich group includes K-ECOC-Nitrate, K-ECOC-Sulfate, K-Secondary and Biomass Burning particles. Potassium had been identified as a good marker for biological sources such as biomass burning, coal burning or plant debris (Creamean et al., 2013). K-ECOC-Nitrate and K-ECOC-Sulfate exhibit intermixing of potassium with carbonaceous fragments ($^{36}C_3^+$, $^{37}C_3H+$, $^{43}C_2H_3O^+$, etc.) or secondary species ($^{97}HSO_4^-$, $^{62}NO_3^-$). ECOC containing particles enriched with potassium and sulfate had been assigned as domestic fuel combustion sources (Dall'Osto et al., 2013), while ECOC-Nitrate, with a larger size mode might associate with transport events (Healy et al., 2012). K-ECOC-Nitrate and K-ECOC-Sulfate varied with diurnal patterns and show good anti-correlation (r = -0.90) with each other. Besides, K-ECOC-Sulfate particles displayed a clear double-mode size distribution as EC particles, while K-ECOC-Nitrate particles mainly distributed in larger size mode. The difference of time variations and diameter distributions implied that K-ECOC-Nitrate possible undergone atmospheric processes. K-Secondary particles are 'deeply aged' particles, featured by unique prominent ion peaks of potassium in positive mass spectra, together with strong intensities of secondary components ($^{46}NO_2^-$, $^{62}NO_3^-$, $^{97}HSO_4^-$, $^{125}H(NO_3)_2^-$) in negative mass spectra.

EC group contains three sub-types, but only the average spectrum of total EC clusters was displayed in Figure S2. Compared with other EC sub-types, NegEC particles show strong ion signal of carbon cluster in negative spectra, especially on $^{24}C_2^-$. Previous researchers
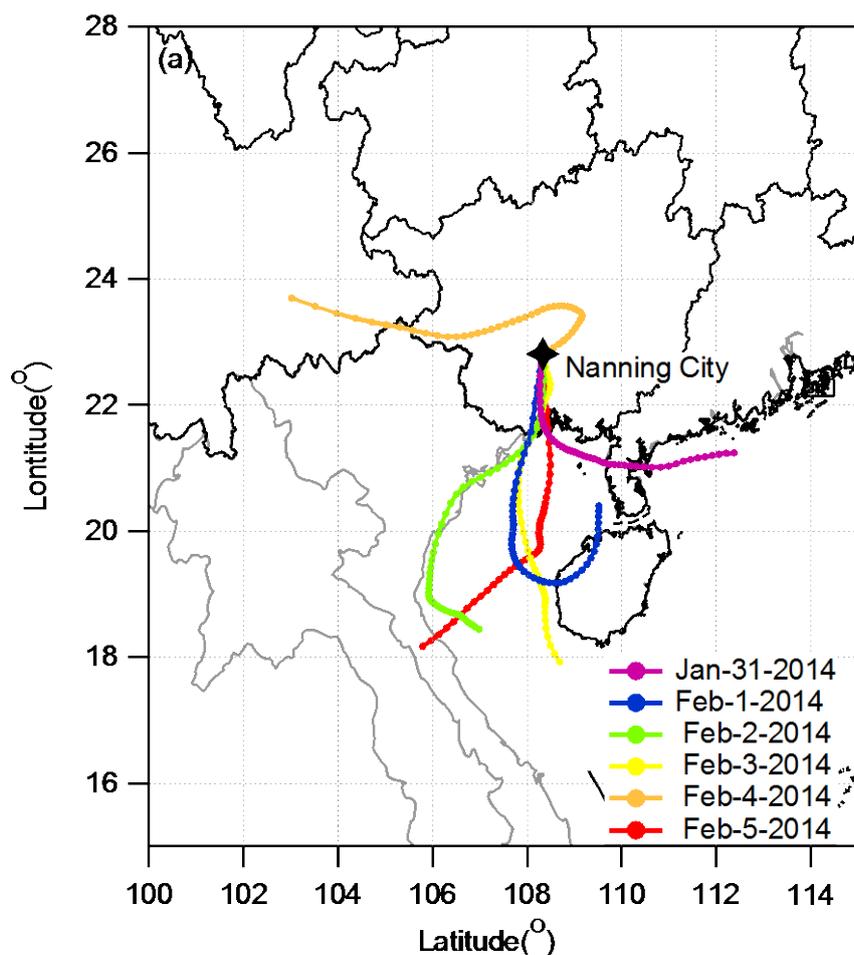
suggested that negative EC peaks are related to primary particles, while positive EC peaks represent aged particles intermixed with secondary species (Giorio et al., 2012; Giorio et al., 2015). K-EC shows comparable intensity between $^{40}K^+$ and $^{36}C_3^+$ ions. The intermixing with sulfate on K-EC particles indicates that this particle type might originate from anthropogenic sources, especially industrial emission (Healy et al., 2012; Chen et al., 2014) or biomass burning emission (Bi et al., 2011). As shown in **Fig. 4**, EC particles exhibited two different size modes. Strong signals of nitrate ($^{46}NO_2$- and $^{62}NO_3^-$) were observed along with large EC particles (Da > 700nm), suggesting that these EC particles were aged with nitrate condensation. Similar results were found in previous single particle observations (Decesari et al., 2014; Zhang et al., 2014).

3. The identification of sulfite on particles

In order to establish a method for identifying sulfite on particles and distinguishing it from sulfate using SPAMS, mass spectra of known compounds were analyzed in laboratory. Solid particles were generated following previously published methods (Silva and Prather, 2000). The solid dry powder of standard compounds (Guoyao Inc, Purity > 99.9%) were firstly suspended by a blender to generate aerosols. After 5 minutes' standing in a sealed glass bottle (to reduce coarse particles), the aerosols were carried by filter air and then analyzed by SPAMS. The standard average mass spectrum of NaCl, K_2SO_4, Na_2SO4 and Na_2SO_3 were generated by the same method. More than 50 individual mass spectrums containing prominent peaks of $^{23}Na^+$ or $^{39}K^+$ were averaged to gain standard mass spectra.

The mass spectrum of NaCl particles was acquired first to verify the feasibility of this method. The clear ion signals of $^{23}Na^{+/-}$, $^{46}Na_2^{+/-}$, $^{35/37}Cl^-$, $^{81/83}Na_2Cl^-$, $^{93/95}NaCl_2^-$, $^{151/153}Na_2Cl_3^-$ were observed in all sodium containing particles (**Fig. S3**). All observed ion clusters were closely related to the ionization of NaCl and no impurities were discovered. As shown in **Fig. S3**, K_2SO_4 and Na_2SO_4 shared similar ion peaks of $^{96}SO_4^-$, $^{80}SO_3^-$, $^{64}SO_2^-$, $^{48}SO^-$, which were sulfur oxide ion clusters of sulfate. Compared with Na_2SO_4, the mass spectrum of Na_2SO_3 displayed prominent signal of $^{80}SO_3^-$ but minor signal of $^{96}SO_4^-$. Even though signal of $^{80}SO_3^-$ also can be generated from sulfate, the relative peak intensities between $^{80}SO_3^-$ and $^{96}SO_4^-$ can be used to tell the difference between sulfite and sulfate containing particles in lab work. Due to ionization features and matrix effect, ions of $^{97}HSO_4^-$ usually appears instead of $^{96}SO_4^-$ in

mass spectra obtained from fieldworks and are commonly chosen as a representative of sulfate (Jeong et al., 2011). Besides, $^{97}HSO_4^-$ also represent organic sulfate in liquid phase (Hatch et al., 2011). Since pure solid samples of inorganic sulfates were used to generate reference spectra in our lab work, weak signals of $^{97}HSO_4^-$ were observed. In order to reflect the sulfate in particulate matter in field research accurately, the sum of relative intensities of $^{96}SO_4^-$ and $^{97}HSO_4^-$ were used to represent total sulfate on particles.
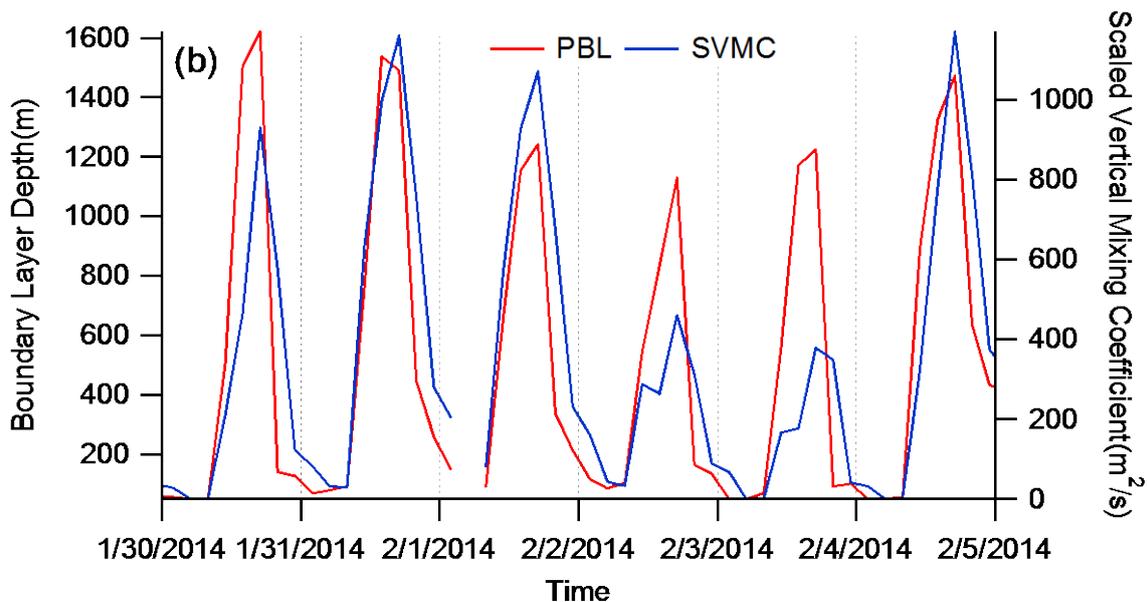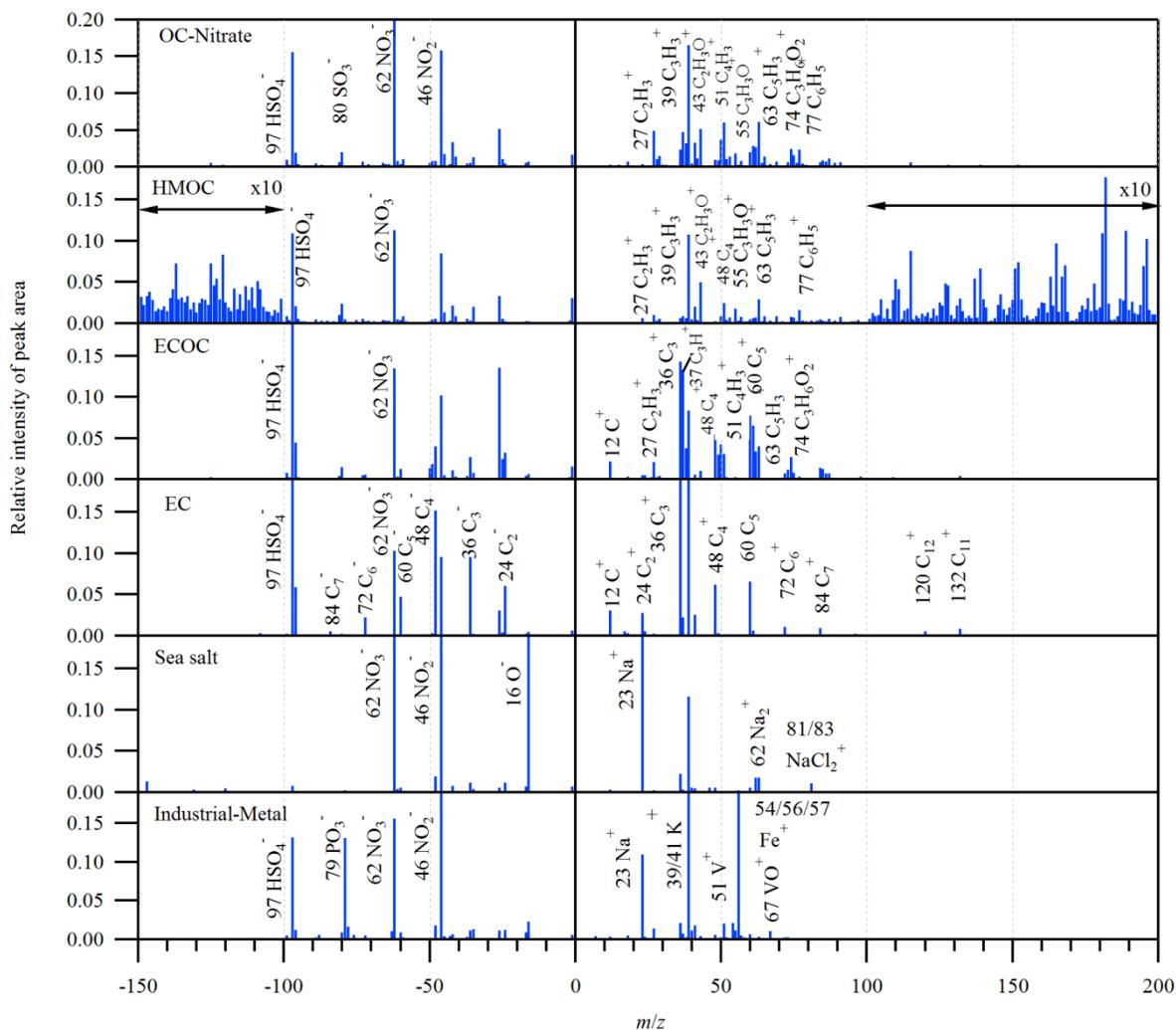
Fig. S1 (a) Air mass back trajectories from 31-Jan-2014 to 5-Feb-2014 (each line represents 48 hours and each point is and average over one hour). (b) Time variation of the stability (PBL and SVMC) of the atmosphere in Nanning from 31-Jan-2014 to 5-Feb-2014.
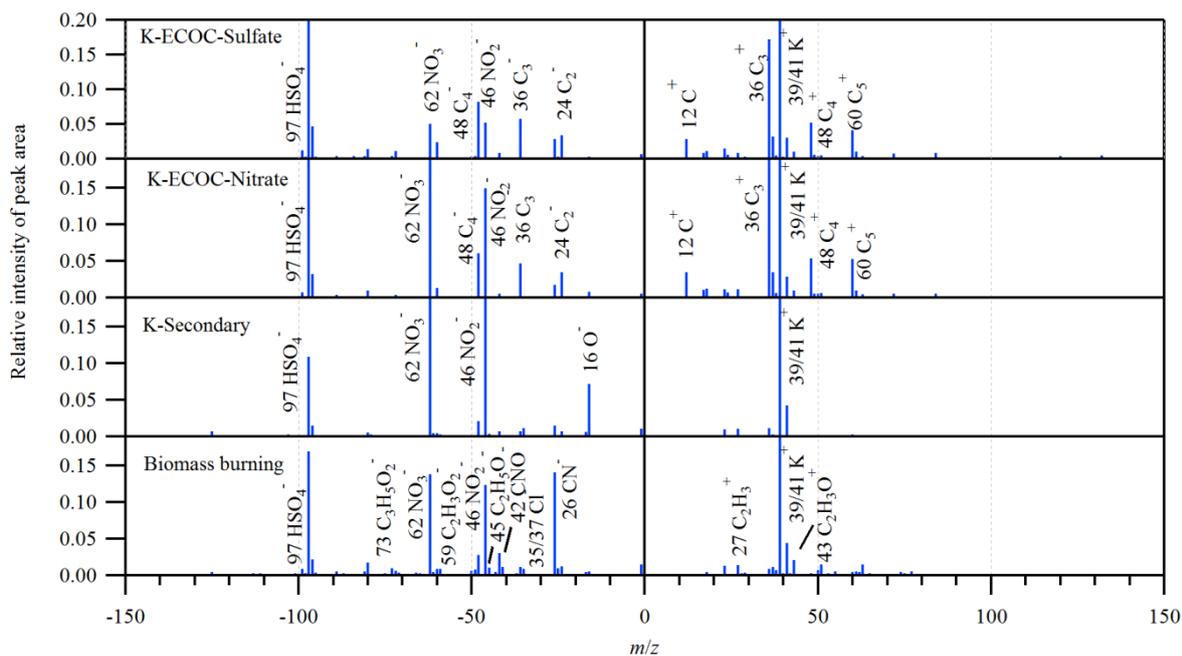
Fig. S2 Average mass spectra of non-firework OC clusters (OC-Nitrate, HMOC) EC, ECOC, Sea salt, Industrial-Metal and K-rich (K-ECOC-Sulfate, K-ECOC-Nitrate, K-Secondary, Biomass Burning) particles. Characteristic *m/z* values used for identification of particle types are marked with possible elemental composition of the ions.
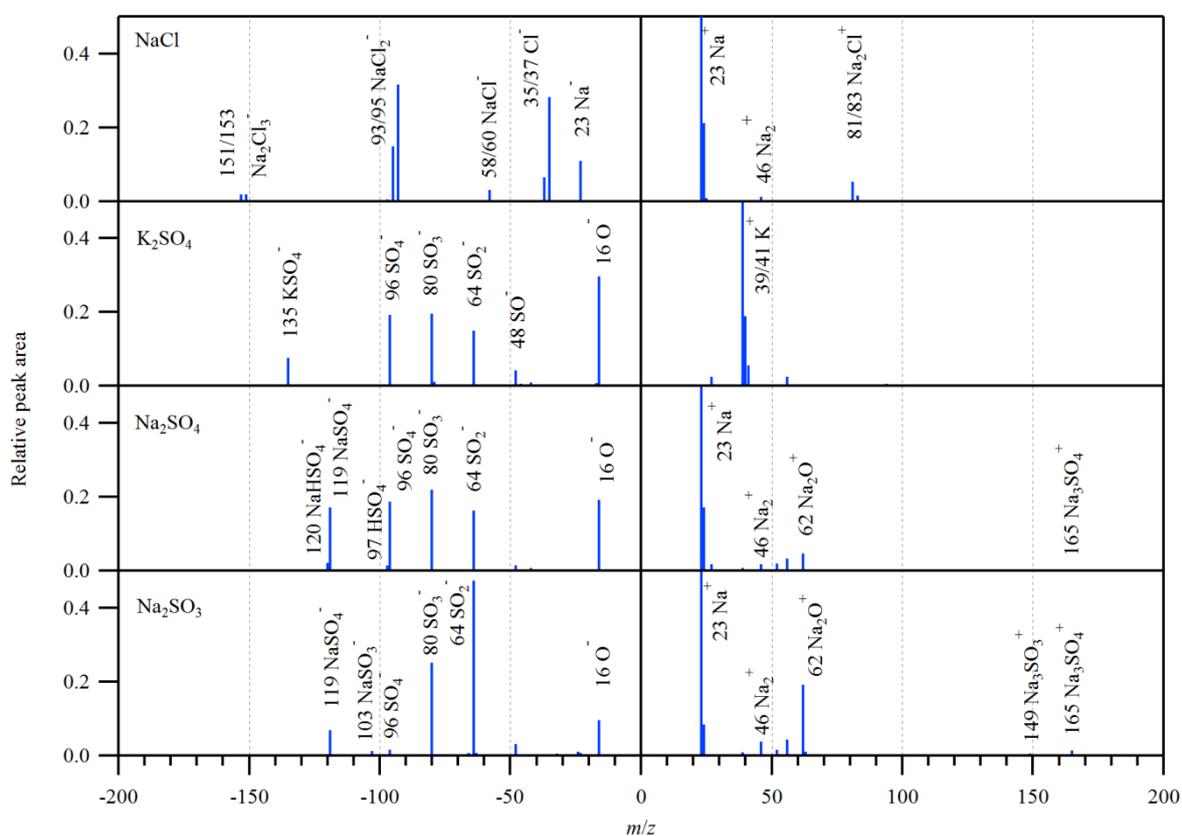
Fig. S3 Average mass spectra gained via lab work. The aerosols were generated by suspending solid powders of NaCl, K_2SO_4, Na_2SO_4 and Na_2SO_3.

References

Bi, X.H., Zhang, G.H., Li, L., Wang, X.M., Li, M., Sheng, G. Y., et al., 2011. Mixing state of biomass burning particles by single particle aerosol mass spectrometer in the urban area of PRD, China. Atmos. Environ. 45(20), 3447-3453.

Camilleri, R. and Vella, A.J., 2010. Effect of fireworks on ambient air quality in Malta. Atmos. Environ. 44(35), 4521-4527.

Chen, K., Yin, Y., Kong, S., Xiao, H., Wu, Y.X., Chen, J.H., et al., 2014. Size-resolved chemical composition of atmospheric particles during a straw burning period at Mt. Huang (the Yellow Mountain) of China. Atmos. Environ. 84(0), 380-389.

Cheng, Y., Engling, G., He, K.B., Duan, F.K., Du, Z.Y., Ma, Y.L., et al., 2014. The characteristics of Beijing aerosol during two distinct episodes: Impacts of biomass burning and fireworks. Environ. Pollut. 185, 149-157.

Creamean, J.M., Suski, K.J., Rosenfeld, D., Cazorla, A., DeMott, P.J., Sullivan, R.C., et al., 2013. Dust and Biological Aerosols from the Sahara and Asia Influence Precipitation in the Western U.S. Science. 339(6127), 1572-1578.

Crespo, J., Yubero, E., Nicolas, J.F., Lucarelli, F., Nava, S., Chiari, M., et al., 2012. High-time resolution and size-segregated elemental composition in high-intensity pyrotechnic exposures. J. Hazard. Mater. 241, 82-91.

Dall'Osto, M., Booth, M.J., Smith, W., Fisher, R. and Harrison, R.M., 2008. A study of the size distributions and the chemical characterization of airborne particles in the vicinity of a large integrated steelworks. Aerosol Sci. Technol. 42(12), 981-991.

Dall'Osto, M., Ovadnevaite, J., Ceburnis, D., Martin, D., Healy, R.M., O'Connor, I.P., et al., 2013. Characterization of urban aerosol in Cork city (Ireland) using aerosol mass spectrometry. Atmos. Chem. Phys. 13(9), 4997-5015.

Decesari, S., Allan, J., Plass-Duelmer, C., Williams, B.J., Paglione, M., Facchini, M.C., et al., 2014. Measurements of the aerosol chemical composition and mixing state in the Po

Valley using multiple spectroscopic techniques. Atmos. Chem. Phys. 14(22), 12109-12132.

Giorio, C., Tapparo, A., Dall'Osto, M., Beddows, D.C.S., Esser-Gietl, J.K., Healy, R.M., et al., 2015. Local and Regional Components of Aerosol in a Heavily Trafficked Street Canyon in Central London Derived from PMF and Cluster Analysis of Single-Particle ATOFMS Spectra. Environ. Sci. Technol. 49(6), 3330-3340.

Giorio, C., Tapparo, A., Dall'Osto, M., Harrison, R.M., Beddows, D.C.S., Di Marco, C., et al., 2012. Comparison of three techniques for analysis of data from an Aerosol Time-of-Flight Mass Spectrometer. Atmos. Environ. 61, 316-326.

Hatch, L.E., Creamean, J.M., Ault, A.P., Surratt, J.D., Chan, M.N., Seinfeld, J.H., et al., 2011. Measurements of Isoprene-Derived Organosulfates in Ambient Aerosols by Aerosol Time-of-Flight Mass Spectrometry - Part 1: Single Particle Atmospheric Observations in Atlanta. Environ. Sci. Technol. 45(12), 5105-5111.

Healy, R.M., Sciare, J., Poulain, L., Kamili, K., Merkel, M., Muller, T., et al., 2012. Sources and mixing state of size-resolved elemental carbon particles in a European megacity: Paris. Atmos. Chem. Phys. 12(4), 1681-1700.

Huang, K., Zhuang, G.S., Lin, Y., Wang, Q., Fu, J.S., Zhang, R., et al., 2012. Impact of anthropogenic emission on air quality over a megacity - revealed from an intensive atmospheric campaign during the Chinese Spring Festival. Atmos. Chem. Phys. 12(23), 11631-11645.

Huo, J.T., Lu, X.H., Wang, X.N., Chen, H., Ye, X.N., Gao, S., et al., 2016. Online single particle analysis of chemical composition and mixing state of crop straw burning particles: from laboratory study to field measurement. Front. Environ. Sci. Eng. 10(2), 244-252.

Jeong, C.H., McGuire, M.L., Godri, K.J., Slowik, J.G., Rehbein, P.J.G. and Evans, G.J., 2011. Quantification of aerosol chemical composition using continuous single particle measurements. Atmos. Chem. Phys. 11(14), 7027-7044.

Joly, A., Smargiassi, A., Kosatsky, T., Fournier, M., Dabek-Zlotorzynska, E., Celo, V., et al., 2010. Characterisation of particulate exposure during fireworks displays. Atmos. Environ. 44(34), 4325-4329.

Kulshrestha, U.C., Rao, T.N., Azhaguvel, S. and Kulshrestha, M., 2004. Emissions and accumulation of metals in the atmosphere due to crackers and sparkles during Diwali festival in India. Atmos. Environ. 38(27), 4421-4425.

Liu, D.Y., Rutherford, D., Kinsey, M. and Prather, K.A., 1997. Real-time monitoring of pyrotechnically derived aerosol particles in the troposphere. Anal. Chem. 69(10), 1808-1814.

McGuire, M.L., Jeong, C.H., Slowik, J.G., Chang, R.Y.W., Corbin, J.C., Lu, G., et al., 2011. Elucidating determinants of aerosol composition through particle-type-based receptor modeling. Atmos. Chem. Phys. 11(15), 8133-8155.

Moffet, R.C., de Foy, B., Molina, L.T., Molina, M.J. and Prather, K.A., 2008. Measurement of ambient aerosols in northern Mexico City by single particle mass spectrometry. Atmos. Chem. Phys. 8(16), 4499-4516.

Moreno, T., Querol, X., Alastuey, A., Minguillon, M. C., Pey, J., Rodriguez, S., et al., 2007. Recreational atmospheric pollution episodes: Inhalable metalliferous particles from firework displays. Atmos. Environ. 41(5), 913-922.

Qin, X.Y. and Prather, K.A., 2006. Impact of biomass emissions on particle chemistry during the California Regional Particulate Air Quality Study. Int. J. Mass spectrom. 258(1-3), 142-150.

Silva, P.J., Liu, D.Y., Noble, C.A. and Prather, K.A., 1999. Size and chemical characterization of individual particles resulting from biomass burning of local Southern California species. Environ. Sci. Technol. 33(18), 3068-3076.

Silva, P.J. and Prather, K.A., 2000. Interpretation of mass spectra from organic compounds in aerosol time-of-flight mass spectrometry. Anal. Chem. 72(15), 3553-3562.

Spencer, M.T., Holecek, J.C., Corrigan, C.E., Ramanathan, V. and Prather, K.A., 2008. Size-resolved chemical composition of aerosol particles during a monsoonal transition period over the Indian Ocean. J. Geophys. Res. 113, D16305.

Sullivan, R.C. and Prather, K.A., 2007. Investigations of the diurnal cycle and mixing state of oxalic acid in individual particles in Asian aerosol outflow. Environ. Sci. Technol. 41(23), 8062-8069.

Tao, S.K., Wang, X.N., Chen, H., Yang, X., Li, M., Li, L., et al., 2011. Single particle analysis

of ambient aerosols in Shanghai during the World Exposition, 2010: two case studies. Frontiers of Environmental Science & Engineering in China. 5(3), 391-401.

Tian, Y.Z., Wang, J., Peng, X., Shi, G.L. and Feng, Y. C., 2014. Estimation of the direct and indirect impacts of fireworks on the physicochemical characteristics of atmospheric PM10 and PM2.5. Atmos. Chem. Phys. 14(18), 9469-9479.

Zhang, G.H., Bi, X.H., He, J.J., Chen, D.H., Chan, L.Y., Xie, G.W., et al., 2014. Variation of secondary coatings associated with elemental carbon by single particle analysis. Atmos. Environ. 92(0), 162-170.